Inorganic Chemistry

Article

pubs.acs.org/IC

Rational Design in Catalysis: A Mechanistic Study of β-Hydride Eliminations in Gold(I) and Gold(III) Complexes Based on Features of the Reaction Valley

Marta Castiñeira Reis,[†] Carlos Silva López,[†] Elfi Kraka,[‡] Dieter Cremer,[*,‡] and Olalla Nieto Faza[*,§]

[†]Departamento de Química Orgánica, Campus Lagoas-Marcosende, 36310 Vigo, Spain

[‡]Computational and Theoretical Chemistry Group, Department of Chemistry, Southern Methodist University (SMU), 3215 Daniel Avenue, Dallas, Texas 75275-0314, United States

[§]Departamento de Química Orgánica, Universidade de Vigo, Campus As Lagoas, 32004 Ourense, Spain

Supporting Information

ABSTRACT: β-Hydride eliminations for ethylgold(III) dichloride complexes are identified as reactions with an unusually long prechemical stage corresponding to the conformational preparation of the reaction complex and spanning six phases. The prechemical process is characterized by a geared rotation of the L−Au−L group (L = Cl) driving methyl group rotation and causing a repositioning of the ligands. This requires more than 28 kcal/mol of the total barrier of 34.0 kcal/mol, according to the unified reaction valley approach, which also determines that the energy requirements of the actual chemical process leading to the β-elimination product are only about 5.5 kcal/mol. A detailed mechanistic analysis was used as a basis for a rational design of substrates (via substituents on the ethyl group) and/or ligands, which can significantly reduce the reaction barrier. This strategy takes advantage of either a higher trans activity of the ligands or a tuned electronic demand of the ethyl group. The β-hydride elimination of gold(I) was found to suffer from strong Coulomb and exchange repulsion when a positively charged hydrogen atom enforces a coordination position in a d^{10}-configured gold atom, thus triggering an unassisted σ−π Au^{I}−C conversion.

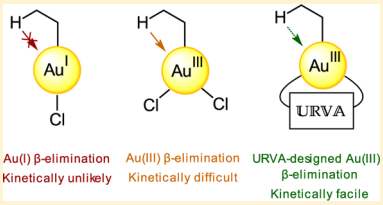

INTRODUCTION

β-Hydride eliminations are frequently used in organometallic chemistry.[1,2] They are typically found in metal alkyl complexes, although they are common in metal alkoxide complexes and other systems and, therefore, have been widely studied both experimentally and theoretically.[3−7] A general objective of these studies is finding a way of suppressing the elimination because it is usually an unwanted byprocess competing with the desired reactions such as cross-coupling, Buchwald−Hartwig amination,[8−11] Ziegler−Natta polymerization, etc.[12−15] However, there are also situations where a β-hydride elimination is a desired reaction, for example, in connection with a chain-walking polymerization[16,17] or the synthesis of metal hydrides.[5,18]

Gold catalysis has flourished in the last 20 years, leading to a wealth of application possibilities.[19−21] The most common catalytic pattern involves cationic gold acting as an extraordinarily mild, yet effective, soft π-acid capable of intra- or intermolecularly activating C−C multiple bonds toward nucleophilic attack.[22,23] Beyond this, there exists an impressive diversity of reactions in which gold catalyzes the assembly of complex molecules via the activation of C−H[24−29] and C−C bonds[29−31] or even cross-coupling reactions.[24,31−34]

The inability of gold to form hydrides and its closely related failure at catalyzing β-hydride eliminations are generally known. These properties are usually considered to be some of the advantages of using gold in catalysis because avoiding β-hydride eliminations reduces the number of undesired processes accompanying catalysis with other metals and often derailing well-planned syntheses. Diatomic Au−H, for instance, could only be detected through codepositon of gold and hydrogen in an argon matrix at 5 K.[35] Nevertheless, the elusive nature of gold hydrides has not deterred chemists from proposing their existence as reactive intermediates,[36] and despite experimental obstacles, the formation of Au−H bonds has been confirmed in complexes with suitably chosen ligands. The first of those to be isolated involved a strongly bound N-heterocyclic carbene ligand to stabilize the labile Au−H interaction.[37] Other gold hydrides have been characterized since then,[38] and the chemistry of gold hydrides has received in the last years increased attention, both experimentally and theoretically,[39,40] focusing on the stability[41] and versatility of these species.[42]

In 2011, Fernández and co-workers[43] reported an astonishing example of gold reactivity in which cyclization of a gold-activated allene was followed by an unexpected gold(III)-catalyzed β-elimination reaction, leading to the formation of a highly strained oxetene. If this catalytic activity could be generalized, it would substantially broaden the scope and applications of homogeneous gold catalysis. Two years later, Köppel and co-workers[44] performed a thorough experimental and computational study that led them to the conclusion that

Received: May 18, 2016
Published: August 18, 2016

DOI: 10.1021/acs.inorgchem.6b01188
Inorg. Chem. 2016, 55, 8636−8645

gold(I) cannot form gold hydrides via a β-elimination of alkylgold complexes. The gold alkene hydride complex produced in this reaction is unstable due to a d^{10} configuration of the gold(I) center, which leads to a high activation barrier that precludes its formation.[45] It is worth noting that the β-hydrogen of a gold(I) complex is known to be hydridic to an extent that it can be abstracted.[45] It is generally accepted that a favorable β-hydride elimination reaction implies that (1) a metal alkyl, alkoxide, or halide has a hydrogen atom in β position to the metal, (2) the metal has an empty coordination site, and (3) the migrating hydrogen is syn-periplanar to the metal. In contrast to gold(I) complexes, conditions (1)−(3) seem to be fulfilled by gold(III) complexes.

This work was triggered by the following findings: (1) gold(I) alkyl complexes are inert toward β-elimination reactions, and very detailed experimental evidence exists that accounts for this behavior;[45] (2) on the contrary, gold(III) has a d^8 electron configuration [valence isoelectronic with palladium(II) and platinum(II)], for which β-hydride eliminations are common;[12,46−52] (3) gold(III)-catalyzed β-hydride eliminations have recently been suggested to occur in a gold complex featuring a highly strained cycloalkyl ligand.[43] Guided by (1)−(3), we performed a detailed mechanistic study of β-hydride eliminations for a variety of gold(I) and gold(III) alkyl complexes to shed light onto the different mechanisms involving gold(I) and gold(III). First, we analyzed the β-elimination step in the system reported by Fernández and coworkers, as depicted in entries c and d of Figure 1 and Table 1.

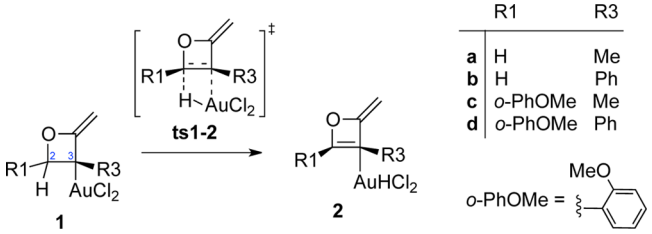

Figure 1. β-Hydride elimination reaction proposed by Fernández et al.[43] as a step in the gold-catalyzed transformation of α-allenols into oxetenes.

Table 1. COSMO(CH_2Cl_2)-DPLNO-CCSD(T)/TZVPP//PCM(CH_2Cl_2)-M06/def2-SVP and PCM(CH_2Cl_2)-M06/def2-SVP Reaction (E_r) and Activation ($E^{\ddagger}$) Electronic Energies (kcal/mol) for the Reactions Depicted in Figure 1

	system		DPLNO-CCSD(T)		M06	
	R1	R3	E_r	$E^{\ddagger}$	E_r	$E^{\ddagger}$
a	H	Me	28.72	30.52	22.32	23.18
b	H	Ph	32.19	33.67	25.27	26.23
c	*o*-PhOMe	Me	13.22	22.32	8.85	17.29
d	*o*-PhOMe	Ph	17.78	26.14	13.50	21.62

Next, we undertook a detailed mechanistic study of the β-elimination reaction of a gold(III) and a gold(I) ethyl complex to provide ethylene and a gold hydride [reactions (R1) and (R2) in Figure 2]. These are the simplest model systems for a β-hydride elimination reaction of a gold complex. The simplicity of the two systems made it possible to analyze the potential energy surfaces (PESs) in a detail that would not be possible for larger systems. We used quantum-chemical methods based on features of the PES to identify those parts

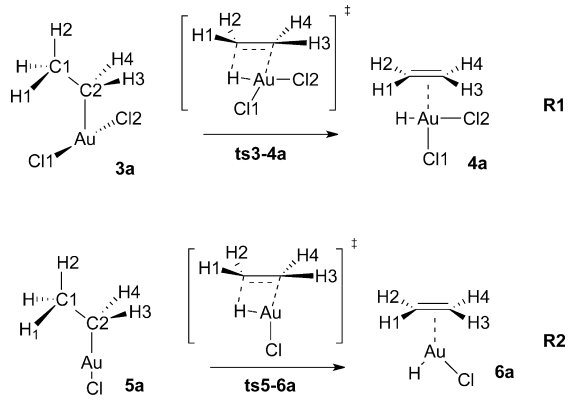

Figure 2. β-Hydride elimination reactions of ethylgold(III) dichloride [reaction (R1)] and ethylgold(I) chloride [reaction (R2)].

of the reaction mechanism that determine the barrier and the features of the system (structural, electronic, electrostatic, etc.) affecting its height. In this way, we have developed a basis to design gold-catalyzed reactions with a lower barrier. We applied the unified reaction valley approach (URVA), which follows the reaction complex (the union of reacting molecules) along the reaction path and registers all changes in its electronic structure to obtain a detailed picture of all chemical events occurring during the chemical reaction.[53−55] The large difference in the barriers between the gold(I) and gold(III)-catalyzed processes made it possible to analyze the role of the oxidation state of the metal, the associated changes in its coordination sphere, and their influence on the reaction mechanism.

The information gathered from this mechanistic study provides a basis to rationally propose and explore structural modifications that could be successful in lowering the reaction barrier, thus providing a convincing example of the possibilities of URVA to design and optimize catalysts for a given reaction.

COMPUTATIONAL METHODS

Quantum-chemical investigation was carried out following a dual-level strategy. The energetics of the reaction was determined utilizing coupled-cluster theory based on all single and double excitations and a perturbative treatment of all triple excitations [CCSD(T)][56] where preliminary density functional theory (DFT) calculations with the M06[57] exchange-correlation functional were used to determine the geometries of the stationary points. For the coupled-cluster calculations, the approximate domain-based local-pair natural-orbital coupled-cluster (DLPNO)[58] approach, as implemented in *ORCA*,[59] has been used.

Unless otherwise stated, DFT investigations were carried out with the def2-SVP basis set of the Ahlrichs group[60] and the ECP-60-MWB pseudopotential for gold.[61] The DLPNO-CCSD(T) calculations were performed with the def2-TZVPP basis set and its associated ECP and auxiliary basis sets for Coulomb fitting procedures.[60,62] Because these organometallic reactions are usually carried out in solution, the effect of solvation has been included in the calculations using implicit models for CH_2Cl_2 at both the DFT and DLPNO-CCSD(T) levels: PCM[63−66] was used in the case of DFT calculations, and COSMO[67] was used when the DLPNO-CCSD(T) energies were computed.

For a reliable account of the reaction mechanism, the PES was calculated and analyzed along the energy valley embedding the reaction path, where the valley was defined by its floor line and the harmonic part of the valley walls in $3N - (L + 1)$ orthogonal directions (N = number of atoms of the reacting molecule; L = number of translations and rotations; plus an additional translation along the path). The curving and winding of the reaction path through the reaction valley reflects the electronic structure changes of the reactant during the reaction.[53−55] This is a direct result of the

DOI: 10.1021/acs.inorgchem.6b01188
Inorg. Chem. 2016, 55, 8636−8645

following: (1) Any electronic structure change is registered by the vibrational normal modes of the reactant. (2) Changes in the normal modes lead to changes in the coupling pattern between molecular vibrations and the translational mode along the reaction path, as reflected by the curvature coupling coefficients.[68] (3) The curvature coupling coefficients determine the curving of the path;[68] (4) The scalar curvature of the reaction path can be decomposed into internal coordinate components,[69] which can be used to identify and characterize the electronic structure changes of the reacting molecule as they relate to bond cleavage (formation), rehybridization, conjugation, charge transfer, etc., where especially the latter can be confirmed by a natural bond orbital (NBO) analysis.[70]

Once the PES has been determined along the reaction valley, analysis of the reaction mechanism is carried out with the URVA method,[53−55] which has already been successfully applied for a series of mechanistic studies.[53,71−75] Each point along the reaction path is characterized in an URVA calculation by its distance from the transition state (TS) given by the arc length s (s = 0 at the TS, with negative values in the entrance channel, s < 0, and positive values in the exit channel, s > 0), the path direction given by the normalized path tangent vector, and the path curvature given by the scalar curvature $\kappa(s)$ that corresponds to the length of the curvature vector $\boldsymbol{\kappa}(s)$. The scalar curvature represented as a function of s has maxima and minima, where the former denote valley regions with distinct electronic structure changes and the latter path regions where the switch from one mechanistic event to the next occurs. We use the minima of the scalar curvature M1, M2, ..., Mn (indicated by dashed vertical lines in the curvature diagrams) to determine the different phases of a reaction (not to be confused with separate reaction steps). This simplifies the description of the reaction mechanism.[53,76] In previous work, curvature minima Mn could be related to *hidden intermediates* and *hidden TSs*, which can become real after suitable changes of the substitution patterns or environmental conditions.[53−55]

In this work, URVA studies were carried out at the DFT level using the B3LYP[77,78] hybrid functional. Although the M06 functional[57] has been shown in several benchmark studies to provide a better description of catalytic cycles involving gold, and transition metals in general,[79−82] it sometimes leads to path instabilities, as reflected by the appearance of imaginary frequencies along the reaction path. Therefore, we have chosen M06 to explore the effects of substitution on the reaction barriers and B3LYP to construct the PES and to perform the subsequent URVA analysis of the reaction path and the reaction valley.

URVA calculations required the use of an ultrafine grid for numerical integrations with 99 radial shells and 590 angular points per shell.[83] For analysis of each reaction valley from its early stages in the entrance channel to the latest stages in the exit channel, calculation of 1000−1400 points along the reaction path were needed where a step size of 0.03 amu$^{1/2}$·bohr (henceforth, denoted as s-units) was employed. Analysis also required as many geometry optimizations of the reaction complex along the path (using *tight* convergence criteria: 10^{-7} hartree/Å) and as many Hessian calculations to obtain normal and local vibrational modes.[84] For calculation of the intrinsic reaction coordinate (IRC), we have used an advanced Hessian-based predictor−corrector integrator,[85] which makes it possible to follow a chemical reaction far out into the entrance and exit channels.[71]

In this work, we analyzed the reaction path curvature in terms of its internal coordinate components because the latter are unaffected by any path instabilities.[69] The stability of the Kohn−Sham wave function was tested for all stationary points (minima and TS) of a given reaction utilizing the procedure of Bauernschmitt and Ahlrichs.[86]

All URVA and local mode calculations were carried out with the program *COLOGNE2016*.[87] For the coupled-cluster calculations, the program *ORCA*[59] was used, whereas DFT calculations were performed with the program *Gaussian09*.[88] Analysis of the atomic charges was done with the *NBO* program of Weinhold and co-workers.[89]

RESULTS AND DISCUSSION

The results of this work will be presented in three sections. The first will briefly explain the computational methodology used because URVA is not yet a mainstream tool in the computational study of reaction mechanisms. This will be followed by a section analyzing the mechanism of the β-hydride eliminations (R1) and (R2) (see Figure 2). The third section summarizes the insights gained from this analysis, which will then be used to propose and test different structural modifications that can lead to an *improved* reaction with lower barriers.

Energetics of the β-Elimination Reaction on the Oxetane Ring. The results of the investigation of the reactions shown in Figure 1 are summarized in Table 1, where, besides the target systems c and d, also the model systems a and b are included for the sake of comparison and to help to determine the effect of the electron-rich aryl group on R1. The energetics calculated for c and d (Table 1; activation free energies of 17.3 and 21.6 kcal/mol, respectively) compare reasonably well with the results obtained by Fernández and co-workers[43] (15.7 and 21.1 kcal/mol). Substitution of a methyl group by a phenyl group on C3 is clearly detrimental to the reaction, as reflected by an increase of the reaction barrier of 3.2−3.8 kcal/mol [DLPNO-CCSD(T) electronic energies]. Conversely, the same reaction without the effect of the *o*-methoxyphenyl group on C2 leads to considerably higher reaction barriers (increase of 7.5 or 8.2 kcal/mol).

The effect of the *o*-methoxyphenyl group on C2 can be explained by better stabilization of the positive charge left by the migrating hydride. However, the effect of substitution on C3 is not as evident and merits further analysis. Therefore, we have carried out URVA analyses of some model reactions for the purpose of answering the question of whether the gold(III)-catalyzed β-elimination can be generalized to other substrates or whether it is restricted to strained oxetanes.

Energetics and a Detailed Mechanistic Study of the β-Elimination Reaction on Simple Alkyl Substituents. A detailed analysis of the energetics of reactions (R1) and (R2) (Figure 2) is summarized in Table 2 and Figure 3. The β-hydride elimination reaction involving ethylgold(III) dichloride [reaction (R1)] is strongly endothermic [DLPNO-CCSD(T), 21.1 kcal/mol; M06, 29.1 kcal/mol] and, accordingly, has a

Table 2. B3LYP/def2-SVP/ECP-60-MWB Gas-Phase Electronic Energies for the Phases in Reactions (R1) and (R2) in kcal/mol (see Figure 2)[a]

	(R1)		(R2)	
phase	contribution	energy	contribution	energy
1	0.7	0.7	2.8	2.8
2	6.0	6.7	0.7	3.5
3	7.8	14.5	5.3	8.8
4	4.4	18.9	22.2	31.0
5	4.0	22.9	42.7	73.7
6	3.5	26.4	−12.2 (2.3)	61.5 (76.0)
7	1.4	27.8	−22.0	39.5
8	5.8	33.6		
9	−2.0 (0.4)	31.6 (34.0)		

[a]For each reaction, the first column indicates the phase's contribution to the reaction barrier and the second column the energy of the reaction complex at the end of the phase. For the phases that include the TS, the energy of the TS is included in parentheses.

DOI: 10.1021/acs.inorgchem.6b01188
Inorg. Chem. 2016, 55, 8636−8645

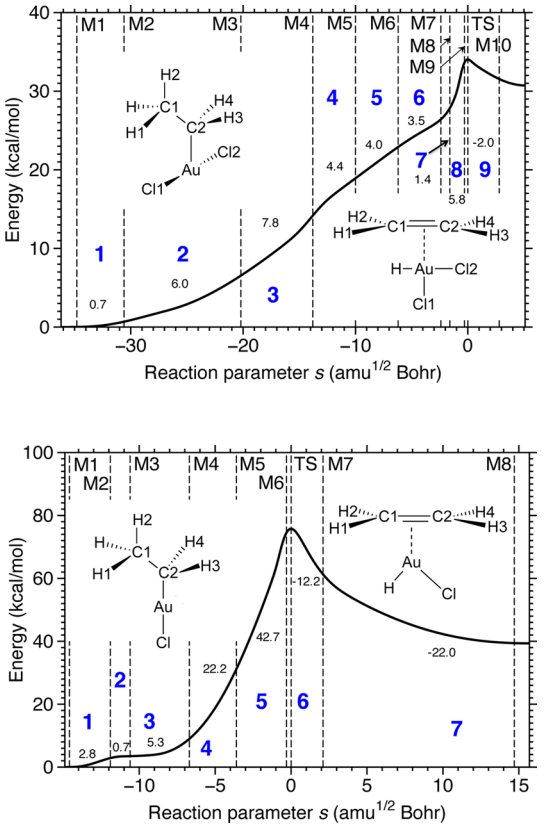

Figure 3. Energy as a function of the reaction path parameter s (solid black line) for the gold(III)-catalyzed β-hydride elimination (R1) (top) and the corresponding gold(I)-catalyzed reaction (R2) (bottom; see Figure 2). Reaction phases (blue numbers) are delimited by vertical dashed lines at curvature minima M1, M2, ..., Mn (Figure 5). The TS at s = 0 amu$^{1/2}$·bohr is also indicated with a vertical dashed line. Small black numbers denote the contribution of each phase to the reaction barrier (in kcal/mol); compare with Table 2. B3LYP/def2-SVP/ECP-60-MWB level of theory.

high barrier [DLPNO-CCSD(T), 21.3 kcal/mol; M06, 30.0 kcal/mol]. As soon as the electron configuration of gold is changed from 5d^8 to 5d^{10}, thus changing gold(III) to gold(I), the β-hydride elimination [reaction (R2)] becomes energetically highly unfavorable, as is reflected by an M06 activation energy of 69.6 kcal/mol [DLPNO-CCSD(T), 72.0 kcal/mol].

According to URVA analysis, reaction (R1) follows a nine-phase mechanism, whereas reaction (R2) is characterized by a seven-phase mechanism (Figures 3 and 5). A summary of the mechanistic features is given in Table 2. A thorough analysis of the most significant features for both mechanisms is provided below.

Mechanism of the β-Hydride Elimination on the Gold(III) System. Reaction (R1) is insofar peculiar as the prechemical phases, in which conformational changes prepare the molecule for the reaction, encompass six phases stretching over almost 34 s-units; i.e., 94% of the entrance channel is needed for the preparation of the reactant before the actual chemical processes take place in phases 7 and 8. The prechemical processes can be characterized by a geared rotation of the σ-bonded Cl−Au−Cl unit driving the methyl group of the ethyl ligand, so that at its end (1) a reactive gold complex with a vacant coordination site is generated, (2) the alkyl substituent is tilted from a σ toward a π kind of interaction with the metal center, and (3) one of the methyl hydrogen atoms is poised to slide as a "hydride" (actually its charge is always slightly positive or neutral; see Figure 4) to the coordination vacancy, where it is led by a buildup of the Au−C1 density. These processes are detailed in the following discussion.

In the reactant **3a**, the linear Cl−Au−Cl unit is oriented perpendicular to the C−C bond to minimize destabilization of eclipsing interactions. In phase 1, the Cl−Au−Cl unit rotates by more than 50° relative to the C−C bond, so that the reactant adopts a sterically less favorable conformation (increase in E, 0.7 kcal/mol; Figure 3, top). This is indicated by the small curvature peak in phase 1 (Figure 5). Stronger changes take place in phase 2, which causes a 6.0 kcal/mol large energy penalty and a second curvature peak at s = −27 units associated with the continued rotation of the alkyl group relative to the Cl−Au−Cl plane (by another 45°) and a bending and tilting (widening of the C2−Au−Cl1 angle by 65°) of this group. The increase in the exchange repulsion between the eclipsed Au−Cl1 and C−C bonds (according to the distance between them) is responsible for the 6.0 kcal/mol raise in energy (Figure 3, top). The curvature components related to the Cl−Au−Cl rotation and angle reduction are all negative, thus indicating that the reactant resists these changes, and energy is needed to overcome this resistance.

In phases 3 and 4, the energy increases by 7.8 + 4.4 = 12.2 kcal/mol, which is 36% of the energy barrier (Figure 3, top). The energy increases almost linearly with the reaction parameter s, which is typical for conformational changes, leading to increasing steric hindrance. Curvature peaks are found at s = −15 units (phase 3) and s = −13 units (Figure 5),

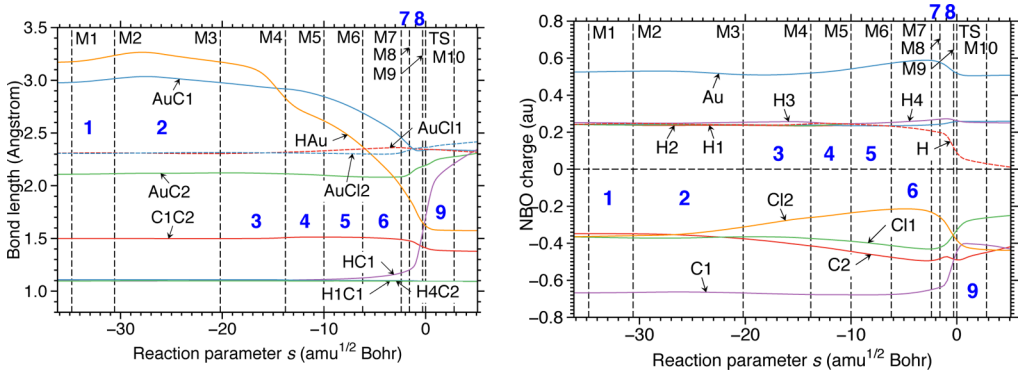

Figure 4. Variation of the key distances (left) and NBO charges (right) as a function of the reaction path parameter s for the gold(III)-catalyzed β-hydride elimination (R1). For the numbering of atoms, see Figure 3. B3LYP/def2-SVP/ECP-60-MWB level of theory.

DOI: 10.1021/acs.inorgchem.6b01188
Inorg. Chem. 2016, 55, 8636−8645

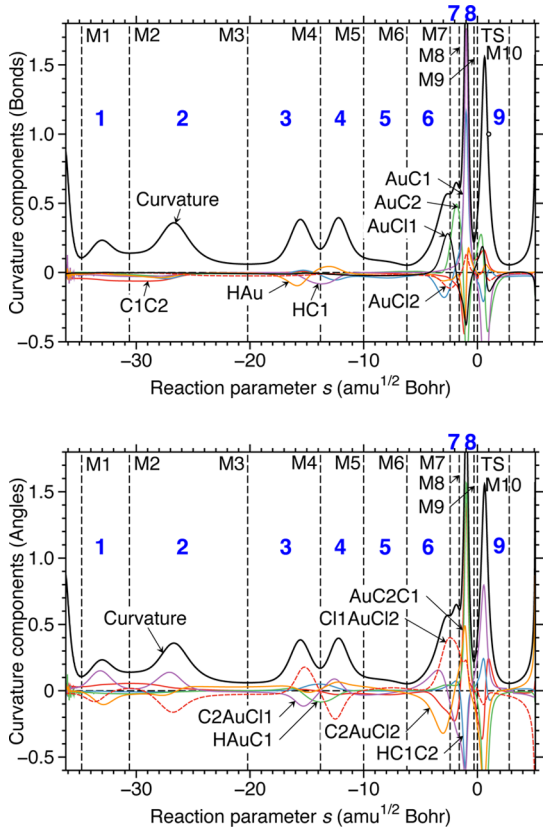

Figure 5. Scalar curvature as a function of the reaction path parameter *s* (solid black line) for the ethylgold(III) *β*-hydride elimination (R1). Curvature components are given in colors (top, bond-length components; bottom, bond-angle components). For the numbering of atoms, see Figure 3. B3LYP/def2-SVP/ECP-60-MWB level of theory.

which are associated with the rotation of the methyl group (in phase 3, resisting the reaction; in phase 4, supporting the reaction) and to a minor extent with the coupled rotation and bending of the Cl−Au−Cl unit. At this point, the C−C−Au angle starts to decrease, thus indicating that, with the geared rotation of the Cl−Au−Cl and methyl units as well as the Cl−Au−Cl angle decrease, the nature of the gold(III) *σ*-complex starts to change. In phase 4, Cl1 (Cl2) becomes more (less) negatively charged as the charge is withdrawn from C2 and, to a lesser extent, from Au to accumulate at Cl1 (Figure 4). This can be explained by the strengthening of the Cl2−Au bond (Figure 4), which becomes trans to a developing vacant coordination site at Au (caused by the reduction of the Cl−Au−Cl angle). The charge relocation in the reacting molecule indicates a differentiation between the two Au−Cl bonds: Cl1 will adopt an axial (trans) position, where it can accumulate more negative charge (Figure 4, right), whereas Cl2 will become an equatorial (cis) ligand with less negative charge.

In phase 5, the linear increase of the energy continues (ΔE = 4.0 kcal/mol). This phase is characterized by conformationally driven (reaction-resisting) C1−Au interactions, which start to develop. Phase 6 follows (ΔE = 3.5 kcal/mol; Figure 5), which is dominated by the Au−C2 adjustment (loss of the *σ*-bond). An agostic Au−H interaction is established, which is characterized by a distance of 2 Å or smaller. After the six prechemical phases, the reactant is ready to undergo changes in bonding; i.e., the chemical processes take place in just two phases (7 + 8) within a short path region of less than 3 *s*-units next to the TS and a final increase in energy of 7.6 kcal/mol. The dominating peak in phase 8 corresponds to the formation of a nonclassical Au−C1 bond and an edge-located hydrogen bridge supporting the Au−C1 interactions (Au−H distance of 1.85 Å or smaller). The dominating peak in phase 9 (shortly after the TS) is associated with cleavage of the nonclassical H−C1 interaction and the coordination of hydrogen to gold via the newly generated coordination vacancy. In these phases, the electrons of the C−C and Au−C2 bonds are delocalized in the Au−C1−C2 unit and are essential for the formation of a *π*-complex between gold(III) and the newly formed ethylene unit in phase 9. In a short postchemical phase, the *π*-complex can adopt its equilibrium geometry.

Mechanism of the β-Hydride Elimination on the Gold(I) System. The reaction has an unusually high barrier of 69.6 kcal/mol at the M06 level of theory, which using DLPNO-CCSD(T) is corrected to 72.0 kcal/mol and thereby of magnitude similar to that of the bond dissociation energy of Au−H (78.4 kcal/mol).[90] The high barrier of (R2) is a direct result of the lack of an empty coordination site in the d^{10} configuration of gold(I) [compared to that in the d^8 configuration of gold(III)]. Clearly, the reaction is of little experimental relevance, as has already been discussed by Köppel and co-workers.[44] However, it nicely shows how the reaction mechanism is changed when gold(III) is replaced by gold(I) with its reduced possibility of coordinating an extra ligand. In the following, we will focus on the mechanistic differences and similarities between reactions (R1) and (R2).

1. Phases 1 and 2. Clearly, reaction (R2) involving gold(I) is mechanistically simpler because there is only one chloride ligand and the geared rotation of the $Au^{III}L_2$ group driving the alkyl rotation is no longer needed. As a result, the number of phases in the mechanism is reduced to 7. Reaction (R2) is initiated by a methyl group rotation in phase 1. The large curvature peak in phase 2 is due to a path bifurcation; i.e., there is a point where a clockwise or counterclockwise rotation of the methyl group can occur, converting a symmetrically staggered conformation into a symmetrically eclipsed one. This brings either H or H1 into a position that is suitable for a hydride transfer to gold(I). The methyl rotation requires 2.8 kcal/mol (phase 1) and leads to a platform of the energy profile (phase 2 in Figure 3). Phase 2 is also the starting point for deformation of the C−C−Au−Cl unit, as indicated by the C−C−Au and C−Au−Cl bond-angle components to the scalar curvature peak (Figure 6).

2. Phases 3−5. The curvature peak in phase 3 at −9 *s*-units gives the onset of formation of a nonclassical Au−C1 interaction (a negative value indicates resistance), which continues to be formed in phase 4 (ΔE = 22.2 kcal/mol) by steady Au−C2−C1 bending and Au−C2 bond weakening requiring 42.7 kcal/mol in phase 5 and leading to a large curvature peak at −1 *s*-units. This is also the position where the H−C1 bond is converted from a classical $2e^-$ bond into a nonclassical one being part of the $2e^-$-3c-bonded C2−C1−H unit. The largest contribution to the barrier (42.7 kcal/mol in phase 5) can be assigned to the establishment of the Au−H interaction in the form of a donor (Au)−acceptor (H) bonding, in which electrostatic repulsion (between two positively charged atoms), besides exchange repulsion, has to be overcome. Once $0.2e^-$ are obtained by hydrogen (from approximately charge 0.2 to 0.0; see Figure 7), reaching the TS in phase 6 requires only an additional 2.3 kcal/mol.

DOI: 10.1021/acs.inorgchem.6b01188
Inorg. Chem. 2016, 55, 8636−8645

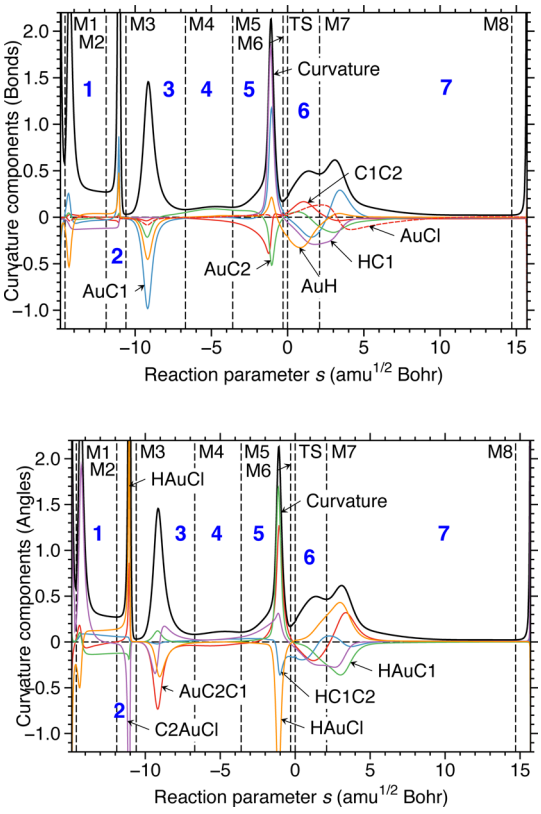

Figure 6. Scalar curvature as a function of the reaction path parameter s (solid black line) for the ethylgold(I) β-hydride elimination (R2). Curvature components are given in colors (top, bond-length components; bottom, bond-angle components). For the numbering of atoms, see Figure 3. B3LYP/def2-SVP/ECP-60-MWB level of theory.

3. Phases 6 and 7. The actual bond finalization steps are all after the TS, as indicated by two broad curvature peaks, one in phase 6 and one in phase 7. The H−Au bonds start to change from a donor−acceptor interaction to a formally dative but strongly covalent ligand−Au bond, which is finalized in phase 7 (Figure 6). The Au−C1 (blue line) and Au−C2 (green line) interactions are converted in two steps into those typical of a π-complex with delocalized 2e$^-$-3c bonding. The C−C bond establishes its double-bond character (red line), the H−C1 bonding interaction is dissolved (phase 7, purple line), and the Au−Cl bond (dashed red component line) gets its final (weakened) form because it has to compete with hydrogen for a suitable coordination site at gold(I), which actually prefers dicoordination rather than tricoordination.

The major difference in the two reactions results from the manner and magnitude of charge transfer to H. In reaction (R1), the transfer of electrons occurs predominantly from C1 to H (0.24e$^-$; apart from another 0.1−0.2e$^-$ transferred from Cl2 and Au to Cl1, the ligand trans to C2). However, in reaction (R2), charge transfer to H is more than twice as large (0.52e$^-$ at the end of the reaction; in phase 6, it peaks at 0.6e$^-$) and involves some charge from C1 and C2, but most of the charge is transferred from Au. Hydride bonding involves in product **4a** an electroneutral hydrogen atom and a strongly positively charged gold(III) (0.5e$^-$), whereas in product **6a**, a strongly negatively charged hydrogen is bonded to a somewhat positive gold(I) (0.3e$^-$). In the energy-consuming phase 5, gold(I) is only slightly charged (0.1−0.2e$^-$). Hence, most of the 22.2 + 42.7 = 64.9 kcal/mol energy contribution of phases 4 and 5 is due to the establishment of Au−C1 and Au−H interactions against charge repulsion.

The evidence collected so far suggests that the reaction can be formally (using the academic arrow-pushing diagrams) described in two steps: (1) The electron pair forming the Au−C2 bond becomes the π-electron pair of the newly formed alkene double bond in phase 5. (2) The electron pair forming the C1−H bond establishes the new Au−H single bond in phase 6. The high energy penalty in phase 5 is due to repulsive interactions between gold and hydrogen atoms that are rapidly becoming negatively charged. In phase 6, the destabilizing interactions convert first into anagostic noncovalent and then into covalent Au−H bonding interactions, thus prompting a further displacement of the chlorine ligand from linearity. This displacement is finalized in phase 7, which is associated with the rearrangement of the ligands at the gold center. There is a decisive change in the H−Au−C1 and C2−Au−Cl angles as the complex adopts its final trigonal geometry.

Because the closed-shell repulsion between the d^{10} gold center and the migrating hydride is the origin of the high energy contribution of 42.7 kcal/mol to the reaction barrier in phase 5, there is little chance of reducing this by changing the structure of the alkyl fragment. This was already demonstrated by Köppel and co-workers.[44] The activation barriers for β-hydride eliminations of some substituted gold(I) alkyl complexes, which confirm this, have been included in the Supporting Information.

Optimization of the Gold(III) System for an Improved β-Hydride Elimination. The β-hydride elimination of gold-

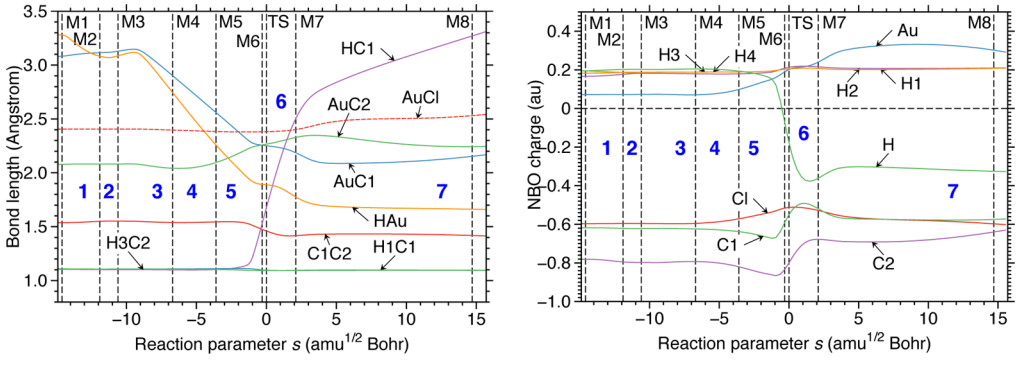

Figure 7. Variation of key distances (left) and NBO charges (right) as a function of the reaction path parameter s for the gold(I)-catalyzed β-hydride elimination (R2). For the numbering of atoms, see Figure 3. B3LYP/def2-SVP/ECP-60-MWB level of theory.

DOI: 10.1021/acs.inorgchem.6b01188
Inorg. Chem. 2016, 55, 8636−8645

(III) complexes is insofar peculiar because the prechemical steps require an unusually high energy amount of more than 28 kcal/mol, whereas the actual chemical processes require just 6.2 kcal/mol. The largely linear increase of the energy in the prechemical phases indicates that, apart from singular electronic effects such as the trans-positioning of Cl2 with regard to the newly developed coordination site at gold(III) or the agostic C−H interaction, there seems to be little chance of reducing the barrier by modifying the reactants investigated. A geared rotation of the Cl−Au−Cl and CH_3 groups coupled with the angle reduction of the former and the positioning of Au above the center of the C−C bond leads to an overall penalty of 28 kcal/mol.

The insight gained by URVA analysis provides guidance on how to reduce the relatively large barrier of 34.0 kcal/mol (B3LYP result, obtained from the IRC calculation). For this purpose, we have focused on reaction phases with large curvature values because these indicate strong electronic structure changes that are associated with a significant energy increase. This applies to phases 3 (7.8 kcal/mol increase; rotation to the C−C−Au−Cl eclipsed form and Cl−Au−Cl bending), 4 and 5 (8.4 kcal/mol; methyl rotation and increased bending), and 8 (5.8 kcal/mol; formation of a nonclassical, hydrogen-bridged gold alkyl complex).

Phases 3−5. These are characterized by an energy penalty of 16.2 kcal/mol, which is associated with the eclipsing of the Au−Cl and C1−C2 bonds and deformation of the Cl−Au−Cl group (apart from the rotation of the methyl group). The changes in the Cl−Au−Cl moiety force Cl1 to adopt a position trans to an alkyl group. Cl1 therefore labilizes the Au−C2 σ-bond and facilitates conversion into a gold(III) π-complex. Chloride is a relatively poor σ-donor and an even poorer π-acceptor. However, both properties are needed to labilize the Au−C2 bond trans-positioned to it (trans effect).[91] Clearly, a cyano ligand has a stronger trans-labilization effect than chloride, and therefore the phase 4 contribution to the activation barrier should be decreased in the presence of this ligand. Accordingly, we calculated the activation barrier for the β-hydride elimination of the ethyldicyanogold(III) and ethylchlorocyanogold(III) complexes **7b** and **7c** (see Figure 8 and Table 3).

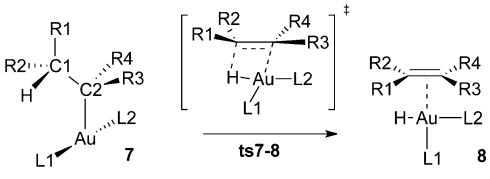

Figure 8. β-Hydride elimination reactions on different substituted ethylgold(III) complexes. The numbering used for ligands corresponds to the entries in Table 3.

The result of these structural modifications of the original gold complex confirms our hypothesis. When only one of the chlorine atoms is replaced (Cl1 in **7c**), the reaction barrier (from now on, we will use DLPNO-CCSD(T) energies, unless otherwise stated) is lowered by less than 1 kcal/mol (Table 3). This modest improvement is due to a balance between the advantage of avoiding the trans interaction between L1 and L2 in phase 4 and the disadvantage of increasing the trans interaction between L1 and C2 in phase 5. The replacement of the second chloride ligand with cyanide in **7b** increases the destabilization of the reactant (due to the two cyanide ligands being trans to each other) and promotes the displacement of L1, thus leading to a lowering of the reaction barrier from 21.3 to 18.5 kcal/mol (entries a and b in Table 3).

Phases 6 and 7. These are not characterized by major electronic structure changes because there are no strong curvature peaks. There is a steady increase in the negative charge at C2, which is accompanied by formation of the Au−C−C−H eclipsed form (via methyl rotation) and the movement of H into a bridge position supported by anagostic interactions. The energy penalty is just 4.9 kcal/mol. Stabilization of the negatively charged C2 can be easily accomplished by using appropriate substituents R3 and R4.

Rather than increasing the trans-directing power of the ligands at gold(III), the strength of the Au−C2 bond can be reduced by withdrawing charge from C2. To test this possibility, we replaced one of the hydrogen atoms at C2 by (1) a fluorine atom, expecting stabilization of the negative charge by inductive electron-withdrawing effects, (2) a formyl group, stabilization through resonance, and (3) a silyl group, stabilization by hyperconjugation with a $\sigma^*(C-Si)$ orbital (see entries d−f in Table 3). Fluorine substitution resulted in a barrier of 26.2 kcal/mol, which is higher than that found for the model system, thus indicating that the π-donation of fluorine outweighs its σ-withdrawing ability. The formyl group reduces the barrier by 0.6 kcal/mol, which can be attributed to an insufficient overlap of the CHO π-orbital and the incipient π(C1−C2) orbital (the O−C−C2−C1 dihedral angle is 155°). The use of a silyl group leads to a 2.1 kcal/mol lowering of the activation energy. This corresponds to a 44% energy reduction with respect to the energy penalty of 4.8 kcal/mol associated with these two phases.

Another possibility to reduce the activation barrier through structural modification is given by the charge depletion at C1 (charge that is transferred to the migrating hydrogen and gold atoms), as found in phases 7 and 8. These phases contribute a total of 7.2 kcal/mol to the reaction barrier. The replacement of hydrogen atoms by phenyl groups, which can stabilize both cations and (to a lesser extent) anions, provides valuable information on the effect of donor and acceptor ligands at C1 and C2. A phenyl ligand at C1 (**ts7-8g**) lowers the barrier from 21.3 kcal/mol in the reference system (**ts7-8a**) to 18.7 kcal/mol, as expected for a donor substituent, whereas the same substitution at C2 (**ts7-8h**) raises the barrier to 24.2 kcal/mol. The latter barrier can be rationalized through the extra stabilization provided to the reactant **7h** with respect to its isomer **7g** (5.7 kcal/mol more stable) or **7a** due to hyperconjugative secondary orbital interactions of the phenyl π-system with the C2−Au bond [NBO analysis: π(Ph) → LP*(C2) and LP*(C2) → π^*(Ph) charge-transfer effects, leading to stabilization of the delocalization energies of −99.2 and −29.0 kcal/mol, respectively]. These two effects combine and cancel each other when both C1 and C2 are substituted with a phenyl group, as in **ts7-8i** and **ts7-8j**. Depending on which direction is chosen for the rotation of the H−C1−C2−Au dihedral angle in **7i** (**7j** has an equivalent structure), the reaction will proceed to the (*E*)- or (*Z*)-alkene complex. In the first case (**ts7-8i**), the barrier barely changes with respect to the reference. In the second case (**ts7-8j**), it is raised by 3.5 kcal/mol because of the steric contacts between the two phenyl groups on the same side of the alkene. The electronic effect of a second phenyl group at C1 is unclear because the activation energy in **7k** is 1.1 kcal/mol higher at the DLPNO-CCSD(T)

DOI: 10.1021/acs.inorgchem.6b01188
Inorg. Chem. 2016, 55, 8636−8645

Table 3. COSMO(CH_2Cl_2)-DPLNO-CCSD(T)/TZVPP//PCM(CH_2Cl_2)-M06/def2-SVP and PCM(CH_2Cl_2)-M06/def2-SVP Reaction (E_r) and Activation ($E^{\ddagger}$) Electronic Energies (kcal/mol) for the Reactions Depicted in Figure 8

	system						M06		DPLNO-CCSD(T)	
	L1	L2	R1	R2	R3	R4	E_r	$E^{\ddagger}$	E_r	$E^{\ddagger}$
a	Cl	Cl	H	H	H	H	29.1	30.0	21.1	21.3
b	CN	CN	H	H	H	H	25.7	27.0	17.7	18.5
c	CN	Cl	H	H	H	H	26.5	29.3	18.4	20.7
d	Cl	Cl	H	H	F	H	−2.7	33.9	24.4	26.2
e	Cl	Cl	H	H	CHO	H	−0.7	30.2	20.2	20.0
f	Cl	Cl	H	H	SiH_3	H	−0.8	28.2	19.4	19.2
g	Cl	Cl	H	Ph	H	H	19.5	24.1	16.3	18.7
h	Cl	Cl	H	H	Ph	H	28.8	32.5	21.7	24.2
i	Cl	Cl	H	Ph	Ph	H	23.7	28.0	18.6	22.0
j	Cl	Cl	Ph	H	Ph	H	29.0	33.0	22.3	24.8
k	Cl	Cl	Ph	Ph	H	H	16.8	22.7	16.9	19.8
l	Cl	Cl	H	H	*p*-NH_2[a]	H	33.6	40.4	29.2	35.2
m	Cl	Cl	H	H	*p*-NO_2[b]	H	29.8	31.2	22.5	23.5
n	Cl	Cl	H	*p*-NH_2	H	H	11.5	21.2	9.5	16.4
o	Cl	Cl	H	*p*-NO_2	H	H	22.2	26.6	17.4	20.2
p	Cl	Cl	H	Me	H	H	20.7	26.0	17.1	18.5
q	Cl	Cl	H	H	Me	H	26.3	29.6	20.9	21.4
r	Cl	Cl	Me	Me	H	H	18.7	21.1	15.7	16.2
s	Cl	Cl	H	NH_2	H	H	−6.6	17.1	−9.1	17.4
t	CN	CN	Me	Me	H	H	16.4	19.3	13.5	14.5

[a] *p*-Aniline. [b] *p*-Nitrophenyl.

level and 1.4 kcal/mol lower at the DFT level (Table 3) with respect to **ts7-8g**.

The hypothesis of charge donation stabilizing charge depletion at C1 in phases 6 and 7 and charge withdrawal stabilizing the increase in the negative charge at C2 in phases 3−5 is further confirmed when the barriers for systems **7g** and **7h** are compared with those corresponding to systems **7l**−**7o**. In these systems, electron-poor and -rich phenyl groups are used by adding strong acceptor (nitro) and donor (amino) substituents in the para position. Thus, the 24.2 kcal/mol barrier that we find for **ts7-8h**, with a phenyl on C2, is raised to 35.2 kcal/mol when its electron-donating properties are enhanced by a *p*-NH_2 group (**ts7-8l**) and decreases to 23.5 kcal/mol when an acceptor such as *p*-NO_2 (**ts7-8m**) is introduced. The opposite trend is observed when the same substitution pattern is applied to C1. In this case, the *p*-NH_2 phenyl substituent significantly lowers the barrier (16.4 kcal/mol, **ts7-8n**), whereas a *p*-NO_2 phenyl substituent raises it to 20.2 kcal/mol (**ts7-8o**).

A similar effect is found when methyl groups are used on C1 and C2 instead of phenyl groups. This is less affected by stabilization of the reactant complex via electronic interactions between the Au−C2 bond or the lone pairs at the chloride ligands and the ethyl substituents. Methyl groups, which can stabilize positive charges through hyperconjugation, barely alter the barrier when located at C2 (**ts7-8o**) but clearly lower the barrier when placed at C1. One methyl group at C1 lowers the barrier by 2.9 kcal/mol with respect to the reference model (**ts7-8p** vs **ts7-8a**). The addition of a second methyl group has in this case a clear amplification effect, and the barrier is further reduced at both the DLPNO-CCSD(T) (by 2.3 kcal/mol) and DFT (by 4.9 kcal/mol) levels (**ts7-8r**).

Because the use of donor substituents at C1 seems to have the largest effect on the reaction barrier, we included **7s** in our study, containing a NH_2 group on C1. The resulting activation barrier for β-hydride elimination (17.4 kcal/mol) is notably lower than the reference value of 21.3 kcal/mol.

To further highlight the use of the URVA method as a tool for systematically designing a reactant that leads to a significantly decreased reaction barrier, we combined the energetically most promising structural modification of the alkyl chain with the best ligand at the metal center among those studied (not a comprehensive study but enough to provide a proof-of-concept). This leads to system **7t** in Table 3, which has a barrier of just 14.5 kcal/mol for the β-hydride elimination reaction.

CONCLUSION

An URVA study of the β-hydride eliminations of ethylgold(III) dichloride complexes has provided a detailed insight into the reaction mechanism. The mechanism has been dissected into nine phases, which have been analyzed and characterized by the following features:

(1) The prechemical phases extend to 34 *s*-units (94% of the entrance channel) and comprise six of the nine phases, leading to the TS. Although all processes taking place in the prechemical phases are conformational in nature, they require 26.4 kcal/mol or 78% of the reaction barrier. This is a consequence of the geared rotation between the ethyl and Cl−Au−Cl groups into a C1−C2−Au−Cl1 eclipsed conformation, which leads to a bending of the linear Cl−Au−Cl moiety and the formation of an axial and an equatorial Cl ligand.

(2) The bending of the Cl−Au−Cl group generates a coordination site for another ligand. At the same time, the axial Cl ligand causes a trans effect, which weakens the C2−Au bond. Methyl group rotation brings one of the CH bonds into a syn-periplanar position.

(3) Once the conformational processes have been carried out, relatively little energy (7.6 kcal/mol) is needed to convert the anagostically interacting C−H bond into a gold hydride, where the latter notation indicates that the positive charge of

DOI: 10.1021/acs.inorgchem.6b01188
Inorg. Chem. 2016, 55, 8636−8645

hydrogen is reduced to zero in the course of the Au−H bond formation. Anagostic/agostic interactions trigger the formation of a nonclassical gold alkene complex.

β-Hydride elimination of gold(I) suffers from Coulomb and exchange repulsion when a positively charged hydrogen atom tries to distort the density of a d^{10}-configured gold(I) atom to generate a suitable coordination site. Accordingly, the activation energy is as high as 70 kcal/mol [DLPNO-CCSD(T)] with the possibility of reducing it to 53 kcal/mol as a result of phenyl substitution.

URVA analysis of the mechanism of β-hydride elimination of ethylgold(III) dichloride was used to design a system for which the barrier of β-hydride elimination is substantially reduced. For this purpose, the focus was on the electronic structure changes of phases 3−8. By considering charge changes during rotation and bending and then enhancing or counteracting these changes by appropriate electron-withdrawing or -donating substituents, a procedure was worked out to reduce the barrier of β-hydride elimination from 21.3 to 14.5 kcal/mol.

Work is in progress to clarify how URVA analysis and the design strategy pursued in this work can be generally applied for the different forms of catalysis.

■ ASSOCIATED CONTENT

Supporting Information

The Supporting Information is available free of charge on the ACS Publications website at DOI: 10.1021/acs.inorgchem.6b01188.

DFT and DLPNO-CCSD(T) energies, Cartesian coordinates and the number of imaginary frequencies for each stationary point, energy profiles, bond-length, bond-angle, and dihedral-angle components to the scalar curvature for each reaction (PDF)

Movie provided for the model reaction, registrating the evolution of the complex along the reaction path (IRC) (MPG)

Movie provided for the model reaction, registrating the evolution of the complex along the reaction path (IRC) (MPG)

■ AUTHOR INFORMATION

Corresponding Authors

*E-mail: dcremer@smu.edu. Phone: +1 (214)768-1300.
*E-mail: faza@uvigo.es. Phone: +34 988 368 888.

Notes

The authors declare no competing financial interest.

■ ACKNOWLEDGMENTS

We thank the Centro de Supercomputación de Galicia for the allocation of computational resources and the Ministerio de Economía y Competitividad for funding (Grant CTQ2013-48937-C2-2-P). C.S.L. and O.N.F. thank the Ministerio de Educación Cultura y Deporte for the financing of their visit to the SMU through the Salvador de Madariaga and José Castillejo programs. M.C.R. thanks the Ministerio de Educación Cultura y Deporte for a predoctoral FPU fellowship. At SMU, this work was financially supported by the National Science Foundation (Grants CHE 1464906 and CHE 1152357). We thank Dr. Freindorf for help with the diagrams and SMU for providing computational resources.

■ REFERENCES

(1) Crabtree, R. H. *The Organometallic Chemistry of the Transition Metals*; John Wiley & Sons, Inc.: New York, 2005; pp 183−206.
(2) Sosa Carrizo, E. D.; Bickelhaupt, F. M.; Fernandez, I. *Chem. - Eur. J.* **2015**, *21*, 14362−14369.
(3) Theofanis, P. L.; Goddard, W. A. *Organometallics* **2011**, *30*, 4941−4948.
(4) Nielsen, R. J.; Goddard, W. A. *J. Am. Chem. Soc.* **2006**, *128*, 9651−9660.
(5) Campbell, A. N.; Gagne, M. R. *Organometallics* **2007**, *26*, 2788−2790.
(6) Schultz, M. J.; Adler, R. S.; Zierkiewicz, W.; Privalov, T.; Sigman, M. S. *J. Am. Chem. Soc.* **2005**, *127*, 8499−8507.
(7) Bryndza, H. E.; Tam, W. *Chem. Rev.* **1988**, *88*, 1163−1188.
(8) Muci, A. R.; Buchwald, S. L. Practical Palladium Catalysts for C−N and C−O Bond Formation. In *Cross-Coupling Reactions: A Practical Guide*; Miyaura, N., Ed.; Springer: Berlin, 2002; pp 131−209.
(9) Wolfe, J. P.; Wagaw, S.; Marcoux, J.-F.; Buchwald, S. L. *Acc. Chem. Res.* **1998**, *31*, 805−818.
(10) Hartwig, J. F. *Acc. Chem. Res.* **1998**, *31*, 852−860.
(11) Hartwig, J. F. *Angew. Chem., Int. Ed.* **1998**, *37*, 2046−2067.
(12) Hao, W.; Wei, J.; Chi, Y.; Walsh, P. J.; Xi, Z. *Chem. - Eur. J.* **2016**, *22*, 3422−3429.
(13) Shrestha, B.; Thapa, S.; Gurung, S. K.; Pike, R. A. S.; Giri, R. *J. Org. Chem.* **2016**, *81*, 787−802.
(14) Curran, K.; Risse, W.; Hamill, M.; Saunders, P.; Muldoon, J.; Asensio de la Rosa, R.; Tritto, I. *Organometallics* **2012**, *31*, 882−889.
(15) Lee, I.; Zaera, F. *J. Phys. Chem. B* **2005**, *109*, 2745−2753.
(16) Hilton, M. J.; Xu, L.-P.; Norrby, P.-O.; Wu, Y.-D.; Wiest, O.; Sigman, M. S. *J. Org. Chem.* **2014**, *79*, 11841−11850.
(17) Tempel, D. J.; Johnson, L. K.; Huff, R. L.; White, P. S.; Brookhart, M. *J. Am. Chem. Soc.* **2000**, *122*, 6686−6700.
(18) Tseng, K.-N. T.; Kampf, J. W.; Szymczak, N. K. *ACS Catal.* **2015**, *5*, 5468−5485.
(19) Pflaesterer, D.; Hashmi, A. S. K. *Chem. Soc. Rev.* **2016**, *45*, 1331−1367.
(20) Wang, Y.; Zhang, L. Gold-calatyzed cascade reactions. In *Catalytic Cascade Reactions*; Xu, P.-F., Wang, W., Eds.; John Wiley & Sons, Inc.: New York, 2013; pp 145−177.
(21) Hashmi, A. S. K.; Rudolph, M. *Chem. Soc. Rev.* **2008**, *37*, 1766−1775.
(22) Zhang, S.; Wei, F.; Song, C.; Jia, J.; Xu, Z. *Chin. J. Chem.* **2014**, *32*, 937−956.
(23) Zi, W.; Dean Toste, F. *Chem. Soc. Rev.* **2016**, DOI: 10.1039/C5CS00929D.
(24) Cambeiro, X. C.; Ahlsten, N.; Larrosa, I. *J. Am. Chem. Soc.* **2015**, *137*, 15636−15639.
(25) Geng, C.; Zhang, S.; Duan, C.; Lu, T.; Zhu, R.; Liu, C. *RSC Adv.* **2015**, *5*, 80048−80056.
(26) Li, Q.; Yang, B.; Lin, H.; Aghdassi, N.; Miao, K.; Zhang, J.; Zhang, H.; Li, Y.; Duhm, S.; Fan, J.; Chi, L. *J. Am. Chem. Soc.* **2016**, *138*, 2809−2814.
(27) Yu, Z.; Qiu, H.; Liu, L.; Zhang, J. *Chem. Commun.* **2016**, *52*, 2257−2260.
(28) Liu, Y.; Yu, Z.; Zhang, J. Z.; Liu, L.; Xia, F.; Zhang, J. *Chem. Sci.* **2016**, *7*, 1988−1995.
(29) Wolters, L. P.; Bickelhaupt, F. M. *Chem. - Asian J.* **2015**, *10*, 2272−2282.
(30) Wegner, H. A.; Auzias, M. *Angew. Chem., Int. Ed.* **2011**, *50*, 8236−8247.
(31) Faza, O. N.; Lopez, C. S. *J. Org. Chem.* **2013**, *78*, 4929−4939.
(32) Hofer, M.; Gomez-Bengoa, E.; Nevado, C. *Organometallics* **2014**, *33*, 1328−1332.
(33) Zhang, G.; Cui, L.; Wang, Y.; Zhang, L. *J. Am. Chem. Soc.* **2010**, *132*, 1474−1475.
(34) Ball, L. T.; Lloyd-Jones, G. C.; Russell, C. A. *J. Am. Chem. Soc.* **2014**, *136*, 254−264.
(35) Wang, X.; Andrews, L. *Angew. Chem., Int. Ed.* **2003**, *42*, 5201−5206.

DOI: 10.1021/acs.inorgchem.6b01188
Inorg. Chem. 2016, 55, 8636−8645

(36) Comas-Vives, A.; González-Arellano, C.; Corma, A.; Iglesias, M.; Sánchez, F.; Ujaque, G. *J. Am. Chem. Soc.* **2006**, *128*, 4756−4765.
(37) Tsui, E. Y.; Müller, P.; Sadighi, J. P. *Angew. Chem., Int. Ed.* **2008**, *47*, 8937−8940.
(38) Roşca, D.-A.; Smith, D. A.; Hughes, D. L.; Bochmann, M. *Angew. Chem., Int. Ed.* **2012**, *51*, 10643−10646.
(39) Crawford, M.-J.; Klapötke, T. M. *Angew. Chem., Int. Ed.* **2002**, *41*, 2269−2271.
(40) Schmidbaur, H.; Raubenheimer, H. G.; Dobrzanska, L. *Chem. Soc. Rev.* **2014**, *43*, 345−380.
(41) Tamaki, A.; Kochi, J. *J. Organomet. Chem.* **1973**, *61*, 441−450.
(42) Roşca, D.-A.; Fernandez-Cestau, J.; Hughes, D. L.; Bochmann, M. *Organometallics* **2015**, *34*, 2098−2101.
(43) Alcaide, B.; Almendros, P.; del Campo, T. M.; Fernandez, I. *Chem. Commun.* **2011**, *47*, 9054−9056.
(44) Klatt, G.; Xu, R.; Pernpointner, M.; Molinari, L.; Hung, T. Q.; Rominger, F.; Hashmi, A. S. K.; Köppel, H. *Chem. - Eur. J.* **2013**, *19*, 3954−3961.
(45) Ung, G.; Bertrand, G. *Angew. Chem., Int. Ed.* **2013**, *52*, 11388−11391.
(46) Martínez-Prieto, L. M.; Ávila, E.; Palma, P.; Álvarez, E.; Cámpora, J. *Chem. - Eur. J.* **2015**, *21*, 9833−9849.
(47) Zhugralin, A. R.; Kobylianskii, I. J.; Chen, P. *Organometallics* **2015**, *34*, 1301−1306.
(48) Takaya, J.; Iwasawa, N. *Chem. - Eur. J.* **2014**, *20*, 11812−11819.
(49) Yang, Y.-F.; Cheng, G.-J.; Liu, P.; Leow, D.; Sun, T.-Y.; Chen, P.; Zhang, X.; Yu, J.-Q.; Wu, Y.-D.; Houk, K. N. *J. Am. Chem. Soc.* **2014**, *136*, 344−355.
(50) Xia, Y.; Ge, R.; Chen, L.; Liu, Z.; Xiao, Q.; Zhang, Y.; Wang, J. *J. Org. Chem.* **2015**, *80*, 7856−7864.
(51) Ellis, C. S.; Ess, D. H. *J. Org. Chem.* **2011**, *76*, 7180−7185.
(52) Konnick, M. M.; Bischof, S. M.; Yousufuddin, M.; Hashiguchi, B. G.; Ess, D. H.; Periana, R. A. *J. Am. Chem. Soc.* **2014**, *136*, 10085−10094.
(53) Kraka, E.; Cremer, D. *Acc. Chem. Res.* **2010**, *43*, 591−601.
(54) Cremer, D.; Kraka, E. *Curr. Org. Chem.* **2010**, *14*, 1524−1560.
(55) Kraka, E. *Wiley Interdisciplinary Reviews: Computational Molecular Science* **2011**, *1*, 531−556.
(56) Raghavachari, K.; Trucks, G. W.; Pople, J. A.; Head-Gordon, M. *Chem. Phys. Lett.* **1989**, *157*, 479−483.
(57) Zhao, Y.; Truhlar, D. G. *Theor. Chem. Acc.* **2008**, *120*, 215−241.
(58) Riplinger, C.; Sandhoefer, B.; Hansen, A.; Neese, F. *J. Chem. Phys.* **2013**, *139*, 134101−13.
(59) Neese, F. *Wiley Interdisciplinary Reviews: Computational Molecular Science* **2012**, *2*, 73−78.
(60) Weigend, F.; Ahlrichs, R. *Phys. Chem. Chem. Phys.* **2005**, *7*, 3297−3305.
(61) Andrae, D.; Häussermann, U.; Dolg, M.; Stoll, H.; Preuss, H. *Theor. Chim. Acta.* **1990**, *77*, 123−141.
(62) Weigend, F. *Phys. Chem. Chem. Phys.* **2006**, *8*, 1057−1065.
(63) Miertuš, S.; Scrocco, E.; Tomasi, J. *Chem. Phys.* **1981**, *55*, 117−129.
(64) Cossi, M.; Barone, V.; Cammi, R.; Tomasi, J. *Chem. Phys. Lett.* **1996**, *255*, 327−335.
(65) Cancès, E.; Mennucci, B. *J. Chem. Phys.* **2001**, *114*, 4744−4745.
(66) Cossi, M.; Scalmani, G.; Rega, N.; Barone, V. *J. Chem. Phys.* **2002**, *117*, 43−54.
(67) Klamt, A.; Schüürmann, G. *J. Chem. Soc., Perkin Trans. 2* **1993**, *2*, 799−805.
(68) Miller, W. H.; Handy, N. C.; Adams, J. E. *J. Chem. Phys.* **1980**, *72*, 99−112.
(69) Zou, W.; Sexton, T.; Kraka, E.; Freindorf, M.; Cremer, D. *J. Chem. Theory Comput.* **2016**, *12*, 650−663.
(70) Weinhold, F.; Landis, C. R. *Valency and Bonding: A Natural Bond Orbital Donor−Acceptor Perspective*; Cambridge University Press: Cambrige, U.K., 2003.
(71) Sexton, T.; Kraka, E.; Cremer, D. *J. Phys. Chem. A* **2016**, *120*, 1097−1111.
(72) Freindorf, M.; Sexton, T.; Kraka, E.; Cremer, D. *Theor. Chem. Acc.* **2014**, *133*, 1423-1−1423-18.
(73) Kraka, E.; Zou, W.; Freindorf, M.; Cremer, D. *J. Chem. Theory Comput.* **2012**, *8*, 4931−4943.
(74) Kraka, E.; Joo, H.; Cremer, D. *Mol. Phys.* **2010**, *108*, 2667−2685.
(75) López, C. S.; Faza, O. N.; Freindorf, M.; Kraka, E.; Cremer, D. *J. Org. Chem.* **2016**, *81*, 404−414.
(76) Kraka, E. In *Wiley Interdisciplinary Reviews: Computational Molecular Science*; Allen, W., Schreiner, P. R., Eds.; Wiley: New York, 2011; pp 531−556.
(77) Becke, A. D. *J. Chem. Phys.* **1993**, *98*, 5648−5652.
(78) Stephens, P. J.; Devlin, F. J.; Chabalowski, C. F.; Frisch, M. J. *J. Phys. Chem.* **1994**, *98*, 11623−11627.
(79) Faza, O. N.; Rodríguez, R. Á; López, C. S. *Theor. Chem. Acc.* **2011**, *128*, 647−661.
(80) Faza, O. N.; López, C. S. Computational Approaches to Homogeneous Gold Catalysis. In *Homogeneous Gold Catalysis*; Slaughter, M. L., Ed.; Springer International Publishing: Cham, Switzerland, 2015; pp 213−283.
(81) Ciancaleoni, G.; Rampino, S.; Zuccaccia, D.; Tarantelli, F.; Belanzoni, P.; Belpassi, L. *J. Chem. Theory Comput.* **2014**, *10*, 1021−1034.
(82) Kang, R.; Chen, H.; Shaik, S.; Yao, J. *J. Chem. Theory Comput.* **2011**, *7*, 4002−4011.
(83) Gräfenstein, J.; Cremer, D. *J. Chem. Phys.* **2007**, *127*, 164113.
(84) Konkoli, Z.; Cremer, D.; Kraka, E. *J. Phys. Chem. A* **1997**, *101*, 1742−1757.
(85) Hratchian, H. P.; Kraka, E. *J. Chem. Theory Comput.* **2013**, *9*, 1481−1488.
(86) Bauernschmitt, R.; Ahlrichs, R. *J. Chem. Phys.* **1996**, *104*, 9047−9052.
(87) Kraka, E.; Zou, W.; Filatov, M.; Gräfenstein, J.; Izotov, D.; Gauss, J.; He, Y.; Wu, A.; Polo, V.; Olsson, L.; Konkoli, Z.; He, Z.; Cremer, D. *COLOGNE16*; 2016.
(88) Frisch, M. J.; et al. *Gaussian 09*, revision D.01; Gaussian Inc.: Wallingford, CT, 2009.
(89) Glendening, E. D.; Reed, A. E.; Carpenter, J. E.; Weinhold, F. *NBO*, version 3.1; Gaussian Inc.: Wallingford, CT, 2009.
(90) Luo, Y.-R. *Handbook of Bond Dissociation Energies in Organic Compounds*; CRC Press: Boca Raton, FL, 2002.
(91) Hartley, F. R. *Chem. Soc. Rev.* **1973**, *2*, 163−179.

DOI: 10.1021/acs.inorgchem.6b01188
Inorg. Chem. 2016, 55, 8636−8645